

Short Communication

Silver Nano-Trees Deposited in the Pores of Anodically Oxidized Titanium and Ti Scaffold

J. Jakubowicz^{1,*}, J.K. Koper¹, G. Adamek¹, M. Połomska², J. Wolak²

¹ Poznan University of Technology, Institute of Materials Science and Engineering, Jana Pawla II 24, 61-138 Poznan, Poland

² Institute of Molecular Physics, Polish Academy of Sciences, Mariana Smoluchowskiego 17, 60-179 Poznan, Poland

*E-mail: jaroslaw.jakubowicz@put.poznan.pl

Received: 9 February 2015 / Accepted: 11 March 2015 / Published: 23 March 2015

The authors present a possibility of growing silver nano-trees in the pits and voids of a titanium surface. The titanium samples used in the experiments were prepared via two different processing paths - by anodic oxidation and powder metallurgy. In the first case a porous Ti oxide surface was formed, whereas in the second case a Ti void composite of the porosity of approx. 70% was formed. Electrochemical deposition using HNO₃ + AgNO₃ mixture leads to a formation of Ag nano-trees that are embedded in the pores. The Ag nano-trees, which are fixed in the pits and voids, should be promising in antibacterial application. The materials were characterized by scanning electron microscopy and Raman spectroscopy.

Keywords: silver nano-trees; deposition; titanium; anodic oxidation; void composite

1. INTRODUCTION

Titanium is one of the most important implant materials providing excellent biocompatibility and mechanical properties for long-life use. In hard tissue implants, rough surfaces improve bonding to the bone, which is why usually a surface treatment is used (anodic oxidation, sand blasting, plasma spraying) in order to generate surface porosity and roughness. Metallic foams, which exhibit overall porosity and high surface roughness, are useful too. Pores in the implants provide anchor points for the bone and ways for body fluid transport (for better angiogenesis). The materials have excellent biocompatibility that assures fast osseointegration, yet, after implantation there is a risk of postoperative bacterial infection. To overcome this problem, a presence of an antibacterial agent on the implant surface is necessary. One of the most effective and safe-to-use agent is silver, which kills most

of the bacteria [1, 2]. Silver, in its metallic state, is inert, however in contact with moisture (body fluid or a wound) takes a highly reactive ionized form.

To provide both osteoblast cells attachment to the implant and bacterial killing, a compromise is necessary, because an excess amount of silver will act against osseointegration. For antibacterial applications, the Ag should come in the form of nanoparticles of large surface area to volume ratio [1]. Smaller particles have a larger surface area to volume ratio, hence, better antibacterial properties. Nanoparticles have been found to be cytotoxic to *E. coli* cells at a concentration of $8 \mu\text{g}/\text{cm}^2$ [2]. For example in [3], the authors used a suspension of Ag nanoparticles to deposit them on the surface during the plasma electrolytic oxidation process.

The synthesis method affects the shape and size of the Ag nanoparticles. For example in [4] the authors applied solvothermal method for the formation of Ag dendrites on the Si single crystal surface. Different methods and processing conditions lead to the formation of Ag dendrites on different materials [5-8], however, to our best knowledge, no one has shown the formation and growth of dendrites in the pores of a porous material.

In the case of porous biomaterials, the pits and pores in the surface act positively not only in terms of cells attachment, but also in terms of antibacterial nanoparticles attachment.

Taking into account the distortions of the electric field at the surface irregularities, as well as structure and composition of the surface layer (usually oxide of different thickness on the top and bottom of the pores) it is suggested that, starting from their bottom, the Ag nanoparticles can grow in the predicted places inside the pores. The best method for controlling the Ag deposition in the pores seems to be electrolytic deposition.

This work presents preferential nucleation and formation of the Ag nano-trees (nanodendrites) in the pores of the anodically oxidized Ti surface and in the pores/voids of the Ti scaffold. The prepared materials will be useful for future hard tissue porous implants showing high level of osseointegration and antibacterial protection.

2. EXPERIMENTAL DATA

In this work porous substrates have been used for Ag nanoparticles deposition made in the following two different processes:

- anodic oxidation applied for the Ti plate. A sample was cut, mechanically grinded and polished using Ti 99.6% rod (Goodfellow); the samples were oxidized in $2\text{M H}_3\text{PO}_4 + 1\text{wt.}\% \text{ HF}$ electrolyte at 210 V for 30 min; more details have been provided in [9],

- powder metallurgy applied for the Ti 99.6% 325 mesh powder (Alfa Easar) as a scaffold material and saccharose particles (table sugar) as a space holder material. They were mixed together and then pressed (1000 MPa) to form a green compact. The saccharose was dissolved in water leaving the air voids surrounded by a solid Ti scaffold. The scaffold was then sintered at $1300 \text{ }^\circ\text{C}$ for 60 min providing a void composite of the porosity of 70%; more details have been provided in [10, 11].

Ag nanoparticles were deposited on the above-mentioned substrates in the form of nano-trees using the electrolytic deposition process. To provide the Ag ions, the aqueous solution of 0.01M

$\text{AgNO}_3 + 0.01\text{M HNO}_3$ was applied. The Ti samples were immersed in the electrolyte and, additionally, an Ag plate (8 cm^2) was used to support the transport of the Ag ions and Ag refilling into the electrolyte. An SCE electrode was used as the reference electrode. EG&G electrochemical cell was applied and the electrolyte inside was mixed using magnetic stirring (250 rpm). The process was controlled by a Solartron 1285 potentiostat. The sample surface area exposed to the electrolyte was 0.8 cm^2 . The Ag nano-trees depositing parameters were as follows: potential -1 V vs OCP (open circuit potential), time 60 s, temperature $20\text{ }^\circ\text{C}$. After deposition, the samples were rinsed in distilled water and dried in a stream of nitrogen.

For the surface analysis Vega Tescan SEM ($U = 20\text{ kV}$) with PGT Prism EDS was applied. Non-polarized Fourier transform near-infrared (FT-NIR) Raman spectra were recorded using a Bruker IFS66FRA106 spectrometer. The samples were excited with a 1064 nm diode-pumped Nd:YAG laser of the output power of 50 mW. The spectra were recorded in the backscattering geometry with 3000 scans and spectral resolution of 4 cm^{-1} . The Raman spectra were measured at the room temperature.

The surface wettability was investigated by measuring the contact angle between the water drop hemisphere and the plane of the sample surface.

3. RESULTS AND DISCUSSION

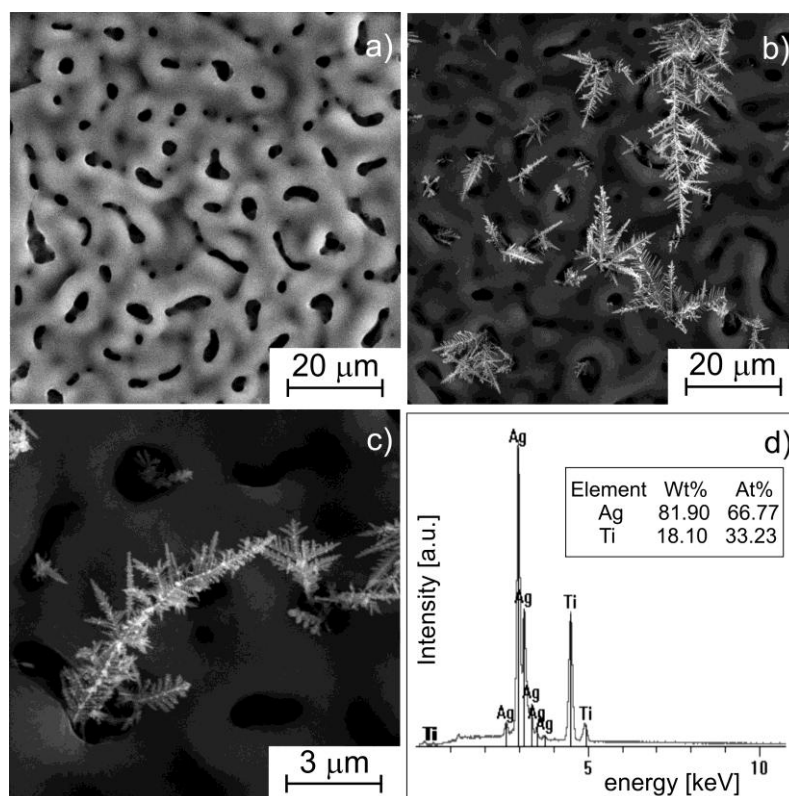


Figure 1. SEM pictures of the anodically oxidized Ti surface (a) and after additional Ag nano-trees deposition (b, c – different magnifications); EDS analysis of the surface covered by the Ag particles (d)

The samples used for the Ag nano-trees deposition process were characterized in previous works by XRD, SEM, AFM and computed tomography (micro-CT) [10-14]. In both cases (anodically oxidized and void composite samples), the two different substrates have surfaces and volume geometrical parameters appropriate for use in hard tissue implants. However, in order to improve their aseptic behavior, silver nanoparticles are deposited on the surface.

The surface roughness of about 0.5 μm and the surface increase (by 10%) for anodically oxidized Ti (Fig. 1a) correspond to the commercially used implant surfaces. The rough oxide porous surface is necessary for the growth and proliferation of the osteoblast cells [12].

The surface morphology of the anodically oxidized Ti and after the deposition of silver is shown on Fig. 1b,c. In the electrolytic deposition process of the Ag nano-trees, the porous substrate that provides necessary surface geometry for nanoparticle nucleation plays the most important role. The surface irregularities such as pits/pores/voids influence the electric field distribution and support the flow of the Ag ions from the electrolyte into the Ti surface. They also influence the nucleation and the initial growth of the Ag nanoparticles. During anodic oxidation, the porous oxides grow from the Ti surface toward the electrolyte. In the bottom of the pits of the anodically oxidized surface, the thickness of the insulating oxide is the thinnest or negligible (corresponding to the native oxide thickness), resulting in a better electric conductivity of the bottom of the pits and a preferential flow of the specific Ag ions. It has been observed that the Ag nanoparticles have a form of nano-trees (nano-dendrites). They start to grow in the surface pits forming main rod-type stem nuclei, from which branched arms oriented at about 60° propagate. The Ag nano-trees have uniform geometry and a relatively large specific surface area, which is required in antibacterial action.

The EDS analysis of the nano-trees precipitations (Fig. 1d) indicates the presence of silver on the sample surface. The nano-trees chemical composition was measured in many points of the dendrites, but due to a relatively large spot of the X-ray beam, the spectrum also shows the Ti substrate (see frame in Fig. 1d). Nevertheless, the Ag peaks dominate in the EDS spectrum.

The characteristics of the Ti-void composites (scaffold) were presented in detail in [10, 11, 14]. Following the micro-CT measurements [14], the sample shown in Fig. 2 has open porosity of approx. 68% and closed porosity of 0.03% only. Hence, the total real porosity is close to the designed porosity of 70%. The average thickness of the solid scaffold is close to 200 μm , while the average structure separation (voids) is close to 350 μm [14].

The electrochemical Ag deposition applied for the sintered Ti scaffold results in a formation of the Ag nano-trees (Fig. 2b) comparable to those formed on the anodically oxidized surface (Fig. 1b, c). The Ti scaffold has relatively large pores defined by the space holder particles (Fig. 2a) that are useful in the osseointegration process. Smaller pores are formed between the sintered Ti particles (Fig. 2b) that are useful for the Ag nano-trees nucleation. During the sintering process, the Ti scaffold undergoes oxidation (despite the fact that sintering was done in protective argon atmosphere), hence the surface is also covered by the oxide [10, 11]. In the scaffold, the silver nanoparticles are fixed in the smaller pores (Fig. 2b) formed between the sintered Ti particles. The Ag nano-trees were found inside and outside of the Ti-void composite sample. The phenomenon is related to free penetration of the electrolyte through the voids in the highly porous structure. In all cases, the Ag nano-trees grow inside the pores.

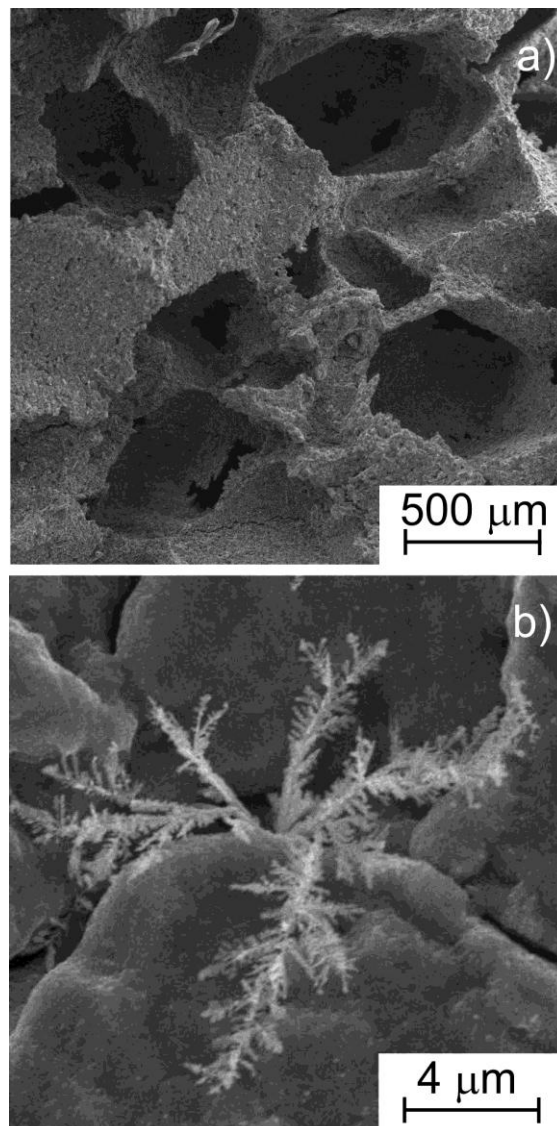


Figure 2. SEM pictures of the Ti-void composite with the deposited Ag nano-trees (a – low magnification; b – large magnification showing the Ag nano-trees position)

In both Ti-type substrates (Fig. 1 and Fig. 2) the Ag nano-trees have a stem diameter of approx. 100–150 nm and the length in the range of 5–100 μm, whereas the length of the arms is in the range of 0.2–20 μm. Wei et al [4] suggest that dendritic silver structures preferentially grow along (111) and (200) directions and, in this method, the structures are 1–2 μm in stem diameter and 10–50 μm in length.

Figure 3 presents the Raman spectra of the anodically oxidized Ti, the Ti void composite, and both surfaces with the Ag nano-trees. The Raman lines were assigned using earlier Raman studies of rutile and anatase structures of TiO₂ [15–18]. The Raman spectrum of the anodically oxidized Ti (Fig. 3a) is more characteristic of the anatase structure of TiO₂. The most intense lines with the E_g symmetry at 146 cm⁻¹ and at 639 cm⁻¹ are well determined in the spectrum. It is rather difficult to determine other lines characteristic of the anatase because of their low intensity. The Raman spectrum of the Ti

void composite (Fig. 3b) consists of two intense lines at 446 cm^{-1} and at 610 cm^{-1} with the E_g and A_{1g} symmetries respectively and a less intense line of the B_{1g} symmetry at 143 cm^{-1} . The broad band centered at about 243 cm^{-1} was reported as related to the multiphonon process in the nano TiO_2 [15]. The Raman spectrum of the Ti void composite corresponds to the rutile structure of TiO_2 .

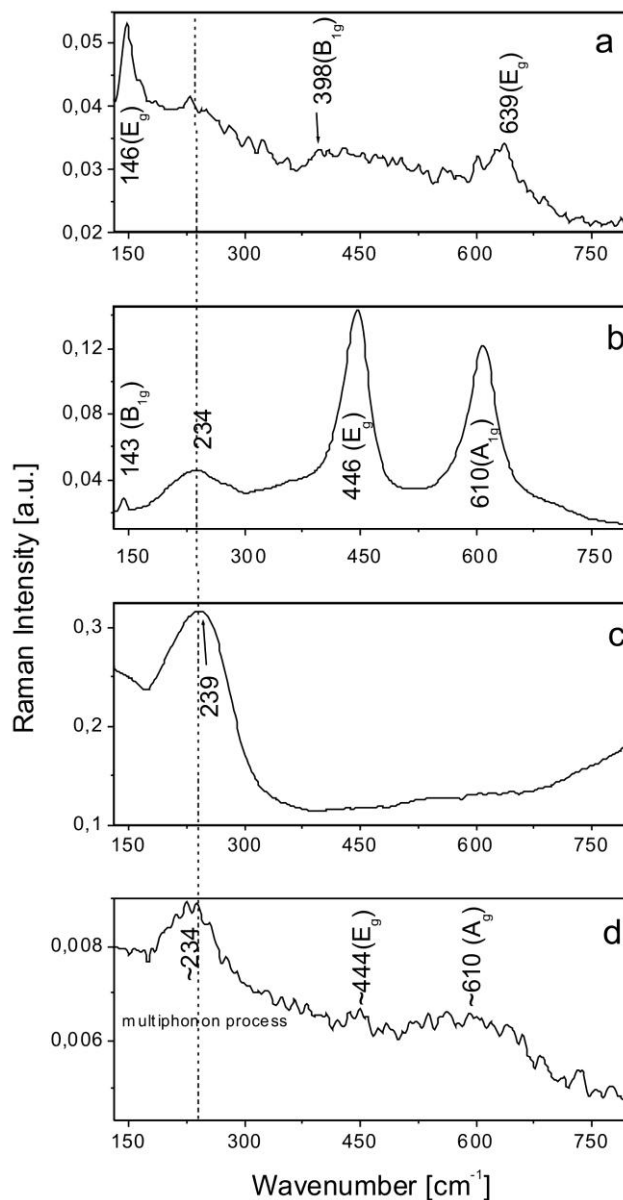


Figure 3. Raman spectra of the anodically oxidized Ti surface (a) and the Ti-void composite after sintering (b), after Ag nano-trees deposition on the anodically oxidized Ti surface (c) and the Ti-void composite (d)

As was presented in Fig. 1 and Fig. 2, both surfaces are useful in the growth of the Ag nano-trees. After Ag deposition, both spectra for the anodically oxidized Ti (Fig. 3c) and the Ti void composite (Fig. 3d) differ significantly from those without the Ag nano-trees. The Ag surface modification enhances scattering at around $230\text{--}239\text{ cm}^{-1}$. This broad band could be related to the

multiphonon process in TiO₂. Moreover, the traces of lines attributed to the rutile form of TiO₂ can also be observed in the Raman spectrum of the Ti void composite with the Ag nano-trees (Fig. 3d). The Raman spectra after Ag deposition indirectly confirm the presence of silver on both surfaces.

The contact angle of the anodically oxidized surface was measured and amounted to $78.7^\circ \pm 5.9^\circ$. After additional silver deposition it increased to $87.9^\circ \pm 4.5^\circ$. This means, that the Ag nano-trees composed of many arms suppress the surface infiltration by water drop, resulting in deteriorating of the hydrophilic properties (cell bioadhesion) and inhibiting the bacterial adhesion. For the Ti scaffold covered by the TiO₂ layer, the contact angle has a comparable value of approx. $87.2^\circ \pm 6.2^\circ$ and does not significantly change after Ag deposition due to the presence of large pores and high surface tension. Dipping of the scaffold in a 10% HF solution for 5 min results in a chemical dissolution of the oxide layer and formation of superhydrophilic surface of the Ti scaffold showing a contact angle approximating 0° (water drop immediately infiltrate the porous scaffold).

4. SUMMARY

In the paper Ag nano-trees (nano-dendrites) electrolytically deposited on the anodically oxidized Ti and on the Ti void composite (scaffold) have been presented. In both cases the Ag nano-trees grew in few-micrometer size pits and pores, where the oxide thickness is negligible, thus supporting the transport of the Ag ions from the electrolyte towards these specific spots in the surface. The Ag nano-trees have a uniform branched symmetry independent of the applied substrate. The made Ag nano-trees should be useful for improving antibacterial behaviour, however respective investigations are needed for the prepared porous biomaterials.

ACKNOWLEDGEMENTS

The work has been financed by National Science Centre Poland under project no. DEC-2012/07/B/ST8/03570.

References

1. X. Chen and H.J. Schluesener, *Toxic. Lett.* 176 (2008) 1.
2. M. Rai, A. Yadav and A. Gade, *Biotechn. Adv.* 27 (2009) 76.
3. B.S. Necula, I. Apachitei, L.E. Fratila-Apachitei, E.J. van Langelaan and J. Duszczuk, *Appl. Surf. Sci.* 273 (2013) 310.
4. Y. Wei, Y. Chen, L. Ye and P. Chang, *Mat. Res. Bull.* 46 (2011) 929.
5. Y. Xia and J. Wang, *Mat. Chem. Phys.* 125 (2011) 267.
6. P.S. Mdluli and N. Revaprasadu, *Mat. Lett.* 63 (2009) 447.
7. Y.-P. Chen, Y. Zhao, K.-Q. Qiu, J. Chu, H.-Q. Yu, G. Liu, Y.-Ch. Tian and Y. Xiong, *Electrochim. Acta* 56 (2011) 9088.
8. B. Rezaei and S. Damiri, *Talanta* 83 (2010) 197.
9. J.K. Koper and J. Jakubowicz, *J. Biomat. Tissue Eng.* 4 (2014) 459.
10. J. Jakubowicz, G. Adamek and M. Dewidar, *J. Porous Mat.* 20 (2013) 1137.
11. G. Adamek, D. Andrzejewski and J. Jakubowicz, *J. Biomat. Tissue Eng.* 4 (2014) 300.

12. J. Jakubowicz, K. Jurczyk and M. Jurczyk, *Mat. Sci. Forum* 636–637 (2010) 15.
13. J. Jakubowicz, G. Adamek, M.U. Jurczyk and M. Jurczyk, *Mat. Character.* 70 (2012) 55.
14. J. Jakubowicz, G. Adamek, K. Pałka and D. Andrzejewski, *Mat. Character.* 100 (2015) 296.
15. H.L. Ma, J.Y. Yang, Y.Dai, Y.B. Zhang, B. Lu, and G.H. Ma, *Appl. Surf. Sci.* 253 (2007) 7497.
16. W. Ma, Z. Lu and M. Zhang, *Appl. Phys. A* 66 (1998) 621.
17. V. Iancu, L. Bala, N. Tarcea, J. Popp and M. Bala, *J. Mol. Str.* 1073 (2014) 51.
18. Y. Xie, Y. Jin, Y. Zhou, and Y. Wang, *Appl. Surf. Sci.* 313 (2014) 549.

© 2015 The Authors. Published by ESG (www.electrochemsci.org). This article is an open access article distributed under the terms and conditions of the Creative Commons Attribution license (<http://creativecommons.org/licenses/by/4.0/>).